



## Article

# Forming Control via Interval Width in Directed Energy Deposition-Arc Process

Qingyuan Wang<sup>1,2</sup>, Zhen Wang<sup>1,2</sup>, Yuhang Xie<sup>1,2</sup>, Jiankang Huang<sup>1,2,\*</sup>, Xiaoquan Yu<sup>3</sup>, Shurong Yu<sup>4</sup> and Ding Fan<sup>1,2</sup>

<sup>1</sup> State Key Laboratory of Advanced Processing and Recycling of Non-Ferrous Metal, Lanzhou University of Technology, Lanzhou 730050, China; wangqy199801@163.com (Q.W.); xyh1997@aliyun.com (Y.X.); fand@lut.edu.cn (D.F.)

<sup>2</sup> School of Materials Science and Engineering, Lanzhou University of Technology, Lanzhou 730050, China

<sup>3</sup> Taizhou Institute of Zhejiang University, Zhejiang University, Taizhou 318000, China; yuxiaoquangood@163.com

<sup>4</sup> School of Mechanical and Electrical Engineering, Lanzhou University of Technology, Lanzhou 730050, China; yushur1991@163.com

\* Correspondence: sr2810@163.com

**Abstract:** A novel controller, employing a variable-structure single-neuron adaptive PSD (proportional integral derivative) approach, was proposed for regulating the deposition width variation in the Directed Energy Deposition-Arc (DED-Arc) layer. During experimental trials, the deposition speed was chosen as the manipulated variable, while the width of the deposition layer served as the measured parameter. To facilitate controller design, a vision sensor was custom-designed to accurately detect the width of the deposition layer. The captured image of the deposition layer's dimensions enabled the precise determination of the deposited thickness, forming the basis for subsequent controller development. In performance assessments, deliberate interference was intentionally introduced into the deposition current, deposition layer height, and the targeted deposition layer width. The assessment involved the controlled deposition of ten-layer components, focusing on width regulation for each deposition layer. The results demonstrate that the proposed controller significantly enhances the deposition process stability, particularly within a range of desired deposition widths from 7.5 mm to 8.3 mm.



**Citation:** Wang, Q.; Wang, Z.; Xie, Y.; Huang, J.; Yu, X.; Yu, S.; Fan, D. Forming Control via Interval Width in Directed Energy Deposition-Arc Process. *Metals* **2024**, *14*, 207. <https://doi.org/10.3390/met14020207>

Academic Editor: Babak Shalchi Amirkhiz

Received: 29 December 2023

Revised: 30 January 2024

Accepted: 6 February 2024

Published: 7 February 2024



**Copyright:** © 2024 by the authors. Licensee MDPI, Basel, Switzerland. This article is an open access article distributed under the terms and conditions of the Creative Commons Attribution (CC BY) license (<https://creativecommons.org/licenses/by/4.0/>).

**Keywords:** DED-Arc; vision sensor; variable layer dimensions; thin-walled components; closed-loop regulating system

## 1. Introduction

Additive manufacturing (AM), also known as 3D printing, is a modern manufacturing technique that centers on the concept of “layer-by-layer stacking” [1,2]. This technology enables the cost-effective production of metal parts and speeds up product development cycles. Metal additive manufacturing technology represents a groundbreaking advancement in advanced manufacturing. It offers an environmentally friendly, efficient, and cost-effective approach to tackle the challenges posed by modern manufacturing technologies. Researchers have explored different heat sources for the additive manufacturing process, such as laser beams [3], plasma or arc [4,5], and electron beams. As a subset of metal additive manufacturing, Directed Energy Deposition-Arc (DED-Arc) utilizes electric arcs to melt and spray material onto the workpiece surface, layer by layer, to build up components [6,7]. The process improves working efficiency [8].

As is widely recognized, the DED-Arc process is a complex and highly interdependent procedure influenced by multiple variables. Changes in individual or combined process parameters inevitably impact the size and quality of the resulting parts. The advancement

of the DED-Arc is hindered not only by these intricate process variables but also by the need for high reliability and automation in engineering applications.

Presently, researchers are primarily focusing on enhancing metal component quality through meticulous process control approaches [9,10]. These approaches encompass off-line modeling and human–computer interaction [11,12], heat accumulation control [13–16], and additive–subtractive composite manufacturing [17–19]. Unfortunately, these methods are predominantly based on non-feedback off-line and open-loop control modes. Implementing online detection and feedback control within the process proves to be a highly effective approach for addressing this challenge. For instance, interlayer temperature can be managed through natural cooling to exert control [20]. Process parameters can be fine-tuned to regulate arc ignition, thus influencing the forming appearance [21]. Moreover, integrating additive manufacturing with milling processes enhances the surface smoothness of the resulting part, thereby elevating its overall quality [22]. However, it remains a challenge to completely eliminate defects using the open-loop control system. From the existing literature, in the effective detection of the geometry of the cladding layer in the DED-Arc, visual sensing is the most convenient detection system. Doumanidis and Kwak [23,24] used active visual perception during multivariate adaptive control, resulting in a detection system which produces a large detection range but not a high accuracy. Heralic et al. [25] applied iterative learning control for the height regulation of laser metal wire deposition.

A Pinot infrared sensing system was created by Fan et al. [26] to keep an eye on the temperature next to the molten pool while arc welding is taking place. This method used the temperature signal that was captured as feedback to control welding penetration. Given the inherent complexity and time-variant nature of arc welding, it is imperative to develop sophisticated control algorithms. Liu and Smith et al. [27] utilized feedback control in Inconel 718's Gas Tungsten Arc welding (GTAW). They utilized a CCD camera to record images of the molten pool surface and assessed the width of the melt pool. This measurement functioned as a feedback signal for controlling the welding process. Zhang [28,29] devised arc welding model-predictive controller procedures with the aim of regulating either penetration or the geometry of the weld pool.

Zhang et al. [30] examined the connection between spectral signals and porosity in the melt deposition process and found that the spectral and electronic intensities were more sensitive to changes in the width of additive molding, which proved the feasibility of spectroscopy for detecting changes in the size of the melt pool. Sangjun Kim et al. [31] estimated the melt pool width, length, depth, and layer height using a single-infrared imaging system. They designed a feedback control system for DED dimensions to enhance the forming quality by adjusting the nozzle movement speed. Hölscher et al. [32], from the University of Hannover, Germany, found that there is a link between the GMAW torch height and the resistance, that the GMAW forming height can be detected by resistance sensing, and that its accuracy can be improved by  $\pm 1.2$  mm. Chabot et al. [33], from the Ecole Centrale de Nantes, France, established a control model between the CMT nozzle height and the acoustic frequency, and the nozzle height can be effectively controlled using this model within a deviation range of 0.5 mm. In the domain of DED-Arc process control, significant research efforts have been directed toward implementing closed-loop control methods. These methods aim to stabilize the forming process, minimize step errors, and reduce defects [34]. The research has predominantly focused on ensuring accuracy in forming geometry and effective thermal control. However, given the complexity of the DED-Arc, characterized by its multiple parameters, nonlinearity, and strong coupling, intelligent control algorithms present a hopeful solution.

In this study, we propose the adoption of a single-neuron self-learning controller. The width of the deposited layer in GTA-AM is chosen as the measured parameter, while the deposition speed functions as the manipulated variable. The primary objective is to attain adjustable width control for each deposition layer in the closed-loop control system for the DED-Arc. Moreover, we aim to extend this capability to control the thickness of

the deposition layer. To evaluate the effectiveness of our proposed control approach, we selected a thin-walled structure fabricated using GTA-AM.

2. Experiment Details

The experimental system manufactured by the arc-added material is mainly composed of Gas Tungsten Arc Welding (GTAW). The welding speed is controlled using a Mitsubishi RV-3SB six-axis robotic arm, serving as both the control end for speed adjustments and the fixed end for the vision sensing system. The visual sensing detection position is illustrated in Figure 1. The power supply is a Panasonic YC200-BL3 constant-current source welding machine (Panasonic, Osaka, Japan). The experimental parameters are shown in Table 1. The tungsten welding torch is fixed on the J6 axis of the robotic arm, maintaining a 5 mm arc length, ensuring the most stable process for metal deposition and forming. When the arc length is 5 mm, GTA-arc combustion is stable, with a moderate height, and there is no occurrence of melting of the deposited metal or adhesion of the tungsten electrode tip. During the welding process, the GTA-arc serves as the heat source to melt the metal wire and substrate. We use 99.99% argon as a shielding gas to prevent the oxidation of the molten pool. The gas flow rate is maintained at 13 L/min. The TC4 metal wire with a diameter of 1.2 mm is employed to deposit metal in this experiment. The TC4 plate with a dimension of 100 mm × 100 mm × 5 mm is selected as the substrate. The composition of the substrate and the welding wire is identical. Table 2 shows the chemical composition of the substrate and the wire. Noteworthy, the deposition current is set to 80 A, without special instructions. Maintaining a consistent distance between the tungsten electrode and the top surface of the deposited layer is essential and so is controlling that the arc pressure is fixed within the feasible range.

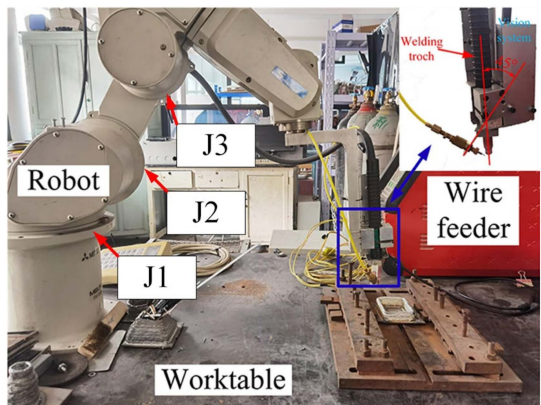


Figure 1. Schematic diagram of the welding system.

Table 1. Basic experimental parameters.

Experimental Parameter	Current	Voltage	Tungsten Electrode	Tungsten Electrode Tip Angle	Tungsten Diameter	Feed Angle	Wire Feed Speed
Numerical value	80 A	11.5 V	WT20	60°	2.4 mm	45°	1.1 m/min

Table 2. Chemical composition of welding wire and substrate (wt %).

Element	Ti	Al	V	Fe	C	N	H	O	Element
Content	Bal	5.99	3.91	0.14	0.014	0.009	0.004	0.17	Content

During the DED-Arc process, it is necessary to ensure that the height from the tip of the tungsten electrode to the top of the cladding layer remains consistent at all times. The robot's movement along the J1, J2, and J3 axes facilitates torch movement in the X, Y, and Z directions, allowing the precise stacking of thin-walled forming components. Once a layer

is completed along the planned path, the arc is extinguished. The J2 axis moves in the Z direction, raising the tungsten electrode by 5 mm, and moves towards the X axis or Y axis to the next arc point, performing the next layer of deposition. In this way, a closed-loop path is formed to avoid excessive accumulation of the arcing end and thermal collapse of the arc's extinguishing end.

Here, the video acquisition device is located to the right of the tungsten electrode, and the DED-Arc real-time deposition process is transmitted through the refraction of the reflector. The specific acquisition equipment is shown in Figure 2. The SG Vision 3.0 software is used for real-time data acquisition. The width of the deposition layer is continually monitored, and the width measurements are recorded using a pixel-based system. Another industrial camera is positioned with a view angle perpendicular to the thin wall and moves in alignment with the deposition speed. The real-time pixels of the thin wall's thickness are collected, and the convex part on the thin wall is detected and avoided. This system is responsible for initiating and terminating the tungsten arc as well as for regulating the wire feed speed and deposition speed. The narrow band filter with a 670 nm wavelength and the passive vision sensor composed of a CCD industrial high-speed camera detect the width and thickness of the sediment layer.

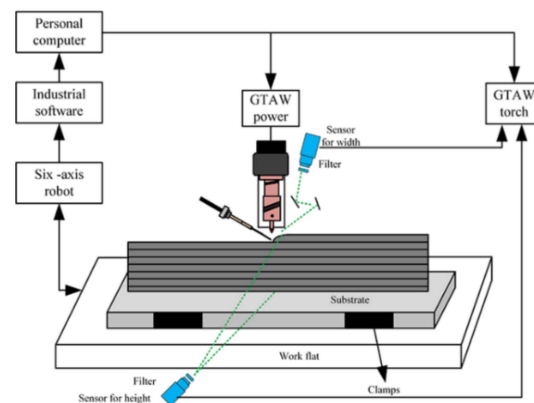


**Figure 2.** Position of the visual sensing system.

The detailed image processing algorithm and program calibration reference [35] image processing flow chart are shown in Figure 3.

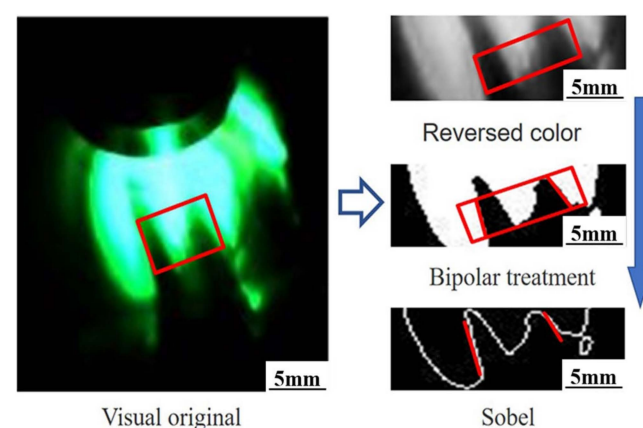


**Figure 3.** Image processing flow chart of the width of the deposit layer developed by MATLAB.

In Figure 3, the real-time acquisition and measurement of the melt pool width by the visual sensor during the additive manufacturing process is depicted. The Sobel operator is a second-order derivative detection operator that is independent of the edge direction, exhibiting isotropic properties and robust noise suppression capabilities. The results after applying the Sobel operator for feature detection on the edges of the image are depicted in Figure 3. From the figure, the boundary of the molten width is clearly observed, with

minimal interference from the edge lines, laying the foundation for extracting the feature values. Due to the presence of noise points or deviations in the edge lines in Sobel edge detection, it is necessary to fit the points on the processed edge lines to accurately locate the width of the deposition layer's edges (depicted by the red line in Figure 3). The selected edge line of the melt pool width is then analyzed to calculate the pixel height of the edge line, converting it into the actual physical width. Additionally, by communicating with the robot's motion trajectory through PLC and CC-Link, real-time control is applied to the movement of the welding gun fixed on the robot's moving joints.

### 3. System Design

To achieve precise process control, a well-designed control system should encompass both the design of control algorithms and the understanding of dynamic characteristics of the control object. A rational control algorithm is fundamental in achieving precise process control, which, in turn, is crucial for producing high-quality formed parts.

Hence, it is essential to develop dynamic models for both control variables. GTA-AM is a complex, multi-variable coupled process. Factors such as deposition speed, wire feed speed, and deposition current significantly influence the final structure formation. To ensure an effective control outcome, we use deposition speed as the manipulated input variable, and the export variable is the width of the deposited layer. To ensure a well-organized test procedure, it is important to conduct a step response test on the input control variables. Among the control variables, the deposition rate has been identified to influence the width of the deposited layer. To clearly observe how the size of the deposited layer changes, a step test is performed on the fourth layer of the single-channel multi-layer deposition by varying the deposition speed. The outcomes of this step test are illustrated in Figure 4. In Figure 4, the Y axis is the width of the deposit layer, and the acquisition time is set as the abscissa of the X axis. Due to the GTA-AM process, where the welding torch is fixed on the robot's J6 and moves along with the axis, the variation in the deposition speed is associated with the movement speed of the robot's J6. As seen in Figure 4, the positive step of the travel speed increases from 1.69 mm/s to 1.98 mm/s, and the negative step of the travel speed decreases from 1.69 mm/s to 1.38 mm/s. It is demonstrated that the travel speed has a negative effect on the layer width. The response of the layer width under the step change has no overshoot. As the deposition speed increases, the width of the deposition layer decreases, indicating a reduction in the amount of melted material entering the molten pool per unit length. Conversely, when the deposition speed decreases, the width of the deposition layer increases. Thus, the DED-Arc can be represented as a first-order transfer procedure, with an expression given by

$$H(s) = \frac{K}{1 + T_s} e^{-\tau s} \quad (1)$$

Here,  $K$  denotes the static amplification factor,  $\tau$  stands for the coefficient representing time delay, and  $T$  signifies the time constant.

Using the discrete system identification algorithms provided by the Matlab language, a mathematical model for a discrete-time dynamic process is obtained. Subsequently, model conversion methods are employed to derive a continuous-time dynamic process mathematical model. Table 3 displays the time constant, gain coefficient, and time delay constant for the deposited layer width in response to positive and negative step changes in the deposition speed.

According to the change trend in Figure 4 and Table 3, it can be found that, when the deposition speed is in a positive step, the rate of welding wire melting is decreased, resulting in a narrower width of the deposition layer. When the deposition speed is in a negative step, the rate of wire melting per unit time increases, which facilitates the increase in the width of the deposition layer.



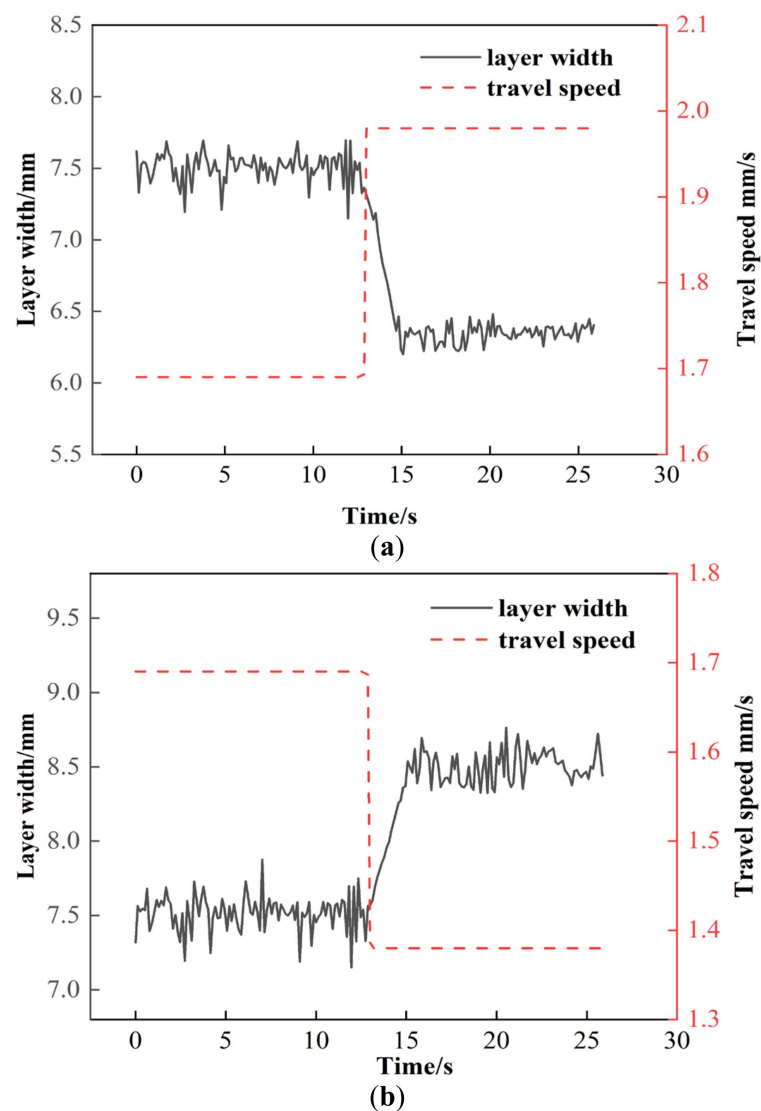


**Figure 4.** The instantaneous effect of sedimentary layer width on speed: (a) positive step, and (b) negative step.

**Table 3.** Time constant, delay, layer width gain coefficient, and travel speed step.

Positive step	K	−0.726
	$T_s$	0.5742
	$T_d$	1.1
Negative step	K	−1.1245
	$T_s$	1.873
	$T_d$	1.4

The findings presented in Table 3 highlight that the width of the deposition layer exhibits the highest gain coefficient during the step response test involving changes in the deposition speed. Furthermore, it is notable that the time constants, gain coefficients, and delay constants of the deposition process differ for positive and negative steps. These discrepancies emphasize that the GTA-AM process is not suitably described by a straight-forward transfer function. To accurately record the trends characteristics of the layer width, a more precise and sophisticated model is essential to represent the intricate trends of the GTA-AM process. After a literature investigation, Xiong et al. [36] employed the nonlinear Hammerstein model to establish trend correlations between the GMAW layer's width and the deposition speed. GTA-AM can use the nonlinear Hammerstein model to represent the

trend relationships between the width of the deposition layer and the deposition speed. Therefore, the system's mathematical representation is as follows:

$$x(k) = C_0 + C_1v(k) + C_2v(k)^2 \quad (2)$$

$$Y(k) = x(k)Z^{-d}B(Z^{-1})/A(Z^{-1}) \quad (3)$$

$Z^{-d}B(Z^{-1})/A(Z^{-1})$ —linear dynamic link

$Y(k)$ —width of the deposited layer

$v(k)$ —walking speed

$Z^{-1}$ —delay operation symbol

$B(Z^{-1})$  and  $A(Z^{-1})$ —polynomial operations

$$A(Z^{-1}) = 1 + a_1Z^{-1} + a_2Z^{-2} + \dots a_nZ^{-n} \quad (4)$$

$$B(Z^{-1}) = 1 + b_1Z^{-1} + b_2Z^{-2} + \dots b_nZ^{-n} \quad (5)$$

where  $n$  is the structural parameter coefficient.

To acquire the suitable input and output data, it is necessary for the deposition speed to fall within a specific range. The deposition speed ranges from 1.69 to 1.92 mm/s, and the speed change trend is shown in Figure 5.

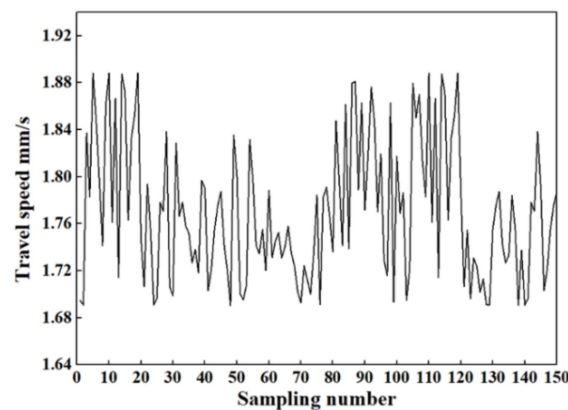


**Figure 5.** Speed change trends of deposition process.

As the robot is a source of motion, the controller has an internal sensor to detect the range of variation in deposition speed. The sensor mainly adopts a continuous trigger mode, and the recorded periodic change time is 0.067 s.

Due to the rapid changes in sensor-recorded data during the GTA-AM process, there is a high density of data points. To manage this, adjustments are made to the data collection start time and delayed collection, considering the short period change time. By calculating the delay constant, we obtain 440 data points in each group and conduct four sets of data tests. Given the challenges posed by single-channel multi-layer stacking, such as high arc end defects, abnormal layer width, and thermal collapse at the tail of a single-channel multi-layer, data from these problematic areas are excluded to ensure data accuracy. In this study, data points are selectively collected from the stable region in the middle. Real-time data are captured using a camera, and the width of the melt pool within the stable region is identified. Through MATLAB programming, the actual width of the melt pool is calculated. The collected data are shown in Figure 6. Correspondingly, Figure 7 illustrates the formation of the single-channel multi-layer structure after data acquisition. Figure 7 demonstrates a smooth and uniform deposition bead without wrinkles, indicating an excellent surface formation quality. This outcome suggests that the fluctuations in deposition current and deposition speed are in a stable state and that the heat input is appropriate.

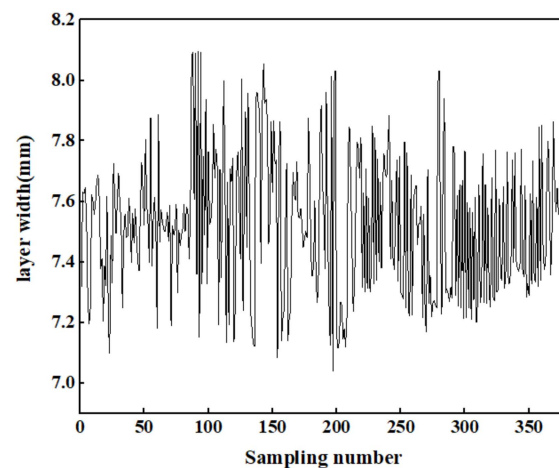


**Figure 6.** Transient response of sediment width under variable deposition rate.

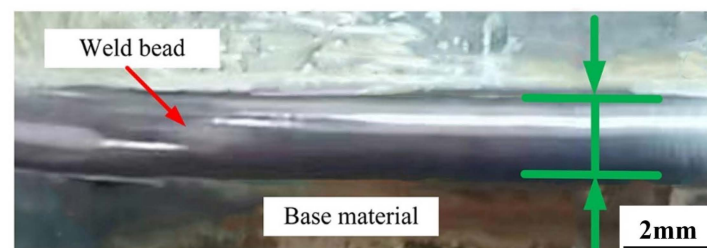


**Figure 7.** Weld macro morphology and size measurement.

It can be observed that the robot has enhanced the stability of the movement source's deposition speed, making the deposition speed change in a stable interval. Then, the input deposition speed first moves briefly at a constant speed and increases or decreases instantaneously within 1 s. The parameters of the Hammerstein model, including  $n = 4$ ,  $b = 4$ , and  $d = 2$ , are determined using the block least squares method. Consequently, the relationship between the deposition speed and the width of the deposition layer during the deposition process of the six-axis robot can be utilized as a representation of the dynamic characteristics:

$$Y(\xi) = 0.275Y\xi - 0.032Y + 0.069 - 0.461v\xi + 1.166v - 0.025v^2\xi - 0.038v^2 \quad (6)$$

#### 4. Controller Design

Given that GTA-AM is a complex, multi-factor, and nonlinear process with numerous variables influencing forming and manufacturing, traditional PID control, being relatively fixed, may not effectively handle this multifaceted manufacturing process. As a result, there is a need for a flexible control algorithm capable of integration with the robot controller through CC-Link, providing the ability for parameter adjustments. This flexibility is vital to efficiently adapt to the diverse and dynamic aspects of the GTA-AM process, allowing for more effective control and optimization of the manufacturing output. Based on a research study from the literature [37], it is found that the variable-structure single-neuron adaptive PSD can complete the expected output and then achieve the desired control effect. By detecting the actual input value and the expected output value, an autonomous learning control is formed.

To optimize the control effect and achieve desirable output values, the backpropagation algorithm is employed to adjust the proportional–integral–derivative (PID) parameters. Following this adjustment, the algorithm influences the deposition process. Simultaneously, a binocular vision sensor is utilized for image acquisition and feature information processing pertaining to the deposition size. The processing procedure is depicted in Figure 3. Within this process, attention is given to collecting and processing data from any defective



sections. Adjustments to the input deposition speed are made accordingly, ultimately influencing the width of the deposited layer. This adaptive approach helps enhance the control and precision of the deposition process, ensuring a more consistent and accurate deposition size and realizing the detection of an actual control effect. The number of inputs can be formulated as follows:

$$\begin{aligned} h_1(t) &= \Delta e(t) = e(t) - e(t-1) \\ h_2(t) &= e(t) \\ h_3(t) &= \Delta^2 e(t) = \Delta h_1(t) = h_1(t) - h_1(t-1) \end{aligned} \quad (7)$$

where the result is due to the output error. The sum of the weights of the three nodes is calculated as follows:

$$o(t) = \sum_{i=1}^3 w_i(t) h_i(t) / \sqrt{\sum_{i=1}^3 w_i^2(t)} \quad (8)$$

To attain a continuous output profile, the S-function is integrated, which leads to an adjustment in the controller's output.

$$\Delta \delta(t) = \delta_{\max} \frac{1 - e^{-o(t)}}{1 + e^{-o(t)}} \quad (9)$$

And, performance indicators can be expressed as follows:

$$J(t) = 0.5 [W_{bset} - W_b(t)]^2 \quad (10)$$

The weight's learning algorithm is computed as follows [38]:

$$\begin{aligned} \Delta w_i(t) &= -\frac{\partial J}{\partial w_i(t)} \\ &= e(t) \frac{\partial W_b(t)}{\partial \Delta \delta(t)} \delta_{\max} \left[ 1 - \frac{\Delta \delta^2(t)}{\delta_{\max}^2} \right] h_i(t) \end{aligned} \quad (11)$$

$$\frac{\partial W_b(t)}{\partial \Delta \delta(t)} \approx \frac{W_b(t) - W_b(t-1)}{\Delta \delta(t) - \Delta \delta(t-1)} \quad (12)$$

The width of the deposited layer in the GTA-AM process is controlled by the PSD control principle, as shown in Figure 8. The input terminal of the controller is determined by the deviation  $W_b$ , which represents the difference between the observed deposited layer width  $W_{set}$  detected by the visual sensor and the predetermined deposited layer width, while the output data correspond to the deposition rate  $v$ . These input and output elements together form a closed-loop control system, regulating the width of the deposition layer during the GTA-AM process.

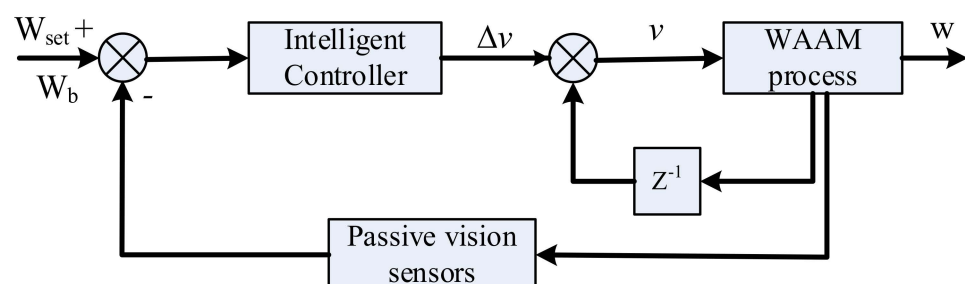


**Figure 8.** Single-neuron self-learning PSD deposition width control schematic in the DED-Arc process.

## 5. Result and Discussion

### 5.1. Control Performance Verification

In this research, the PSD control algorithm is used to control the equal width of the lightweight structure's structural parts manufactured by the robot GTA-AM. In simple

terms, maintaining a consistent layer width for structural components in the DED-Arc involves regulating the separation amid the tungsten electrode and the surface at the deposition layer's top, in addition to adjusting other critical process parameters. To verify that the designed PID control algorithm is correct, simulation experiments are essential. These simulations help validate the control algorithm's capability to achieve the desired and uniform layer width in the manufactured components. The simulation experiment is realized using the MATLAB language, and the simulated unit neural control result curve is shown in Figure 9.

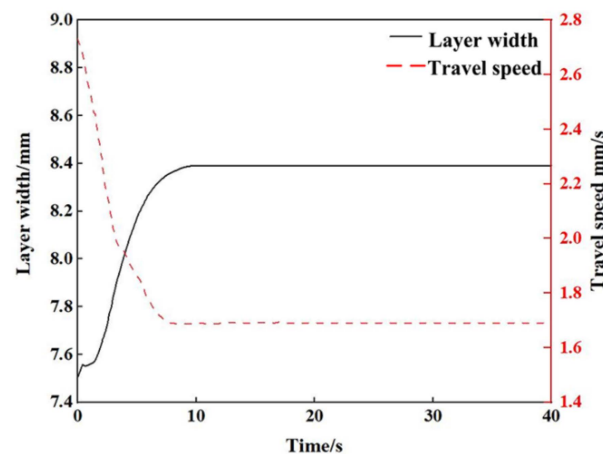


**Figure 9.** Simulation detection curve of single-neuron control system.

When employing the MATLAB language, the initial width of the deposited layer is established at 7.5 mm, and the deposition speed is adjusted to 2.65 mm/s. In the course of the simulation test, the deposition rate decreases to 1.69 mm/s. The anticipated step value for the cladding layer width is 8.3 mm. The simulation results align precisely with the anticipated control effect expected for the test. This congruence underscores the effectiveness of the simulation in accurately representing and predicting the behavior of the deposition process in response to changes in the deposition speed. To verify the authenticity of the experimental simulation, we set the deposition speed as constant. Considering that the speed change at the corner is caused by the angle operating mechanism of the robot, the deposition width and deposition speed change noticeably at the corner, and only data recorded when the sediment layer is relatively stable and the speed of movement is stable are considered. Figure 10 depicts the experimental results. It is observed that the time required for the speed to stabilize is 9 s, aligning with the simulation outcomes.

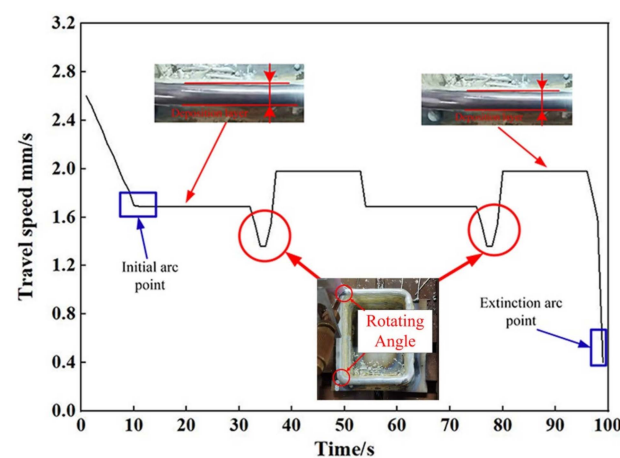


**Figure 10.** Rotational angular speed and constant speed in the deposition process.

To ensure the practical application of the PID control, interference tests are designed specifically for controlling the width of the deposited layer. These tests consist of a closed-loop disturbance test within a designated width range, as shown in Figure 11, and a closed-loop control test subjected to steps of the sedimentary current, as shown in Figure 12. The width of the deposited layer detected by the visual sensor is referred to as “ $W_b$ ”, while “ $W_{set}$ ” is the predetermined deposition layer width. Given that the sensor used in this study has a continuous acquisition time of 0.06 s, it effectively collects 16 data points in 1 s. By utilizing these data points, the trend in the change in the deposited layer’s size is calculated. The significant change in width occurs when the cladding layer size increases from 7.5 mm to 8.3 mm at approximately  $t = 15$  s. Through PSD control, the width of the deposited layer stabilizes, taking approximately 4 s to 5 s for this stabilization to occur. Post stabilization, the visual sensor is used for re-detection. The width of the new cladding layer falls within the range of 8.1 mm to 8.5 mm after detection by the visual sensor. If the width of the new cladding layer falls within this range of change, it is deemed normal. Additionally, it is imperative to measure the maximum error between the width and height of the layer, and the designated layer width does not exceed 0.8 mm, ensuring the precise control and validation of the PSD control’s practicality in maintaining the desired layer width.

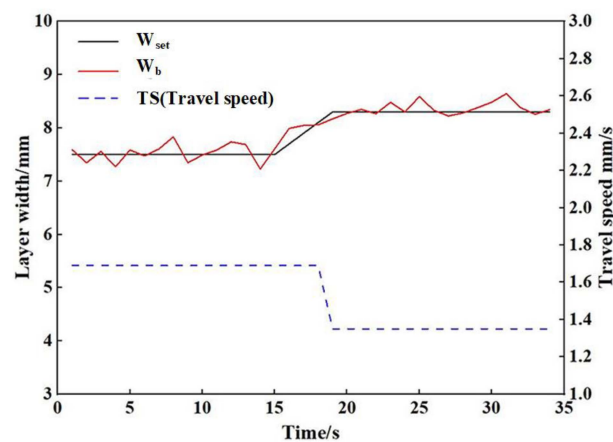


Figure 11. Closed-loop control disturbance for given width range.

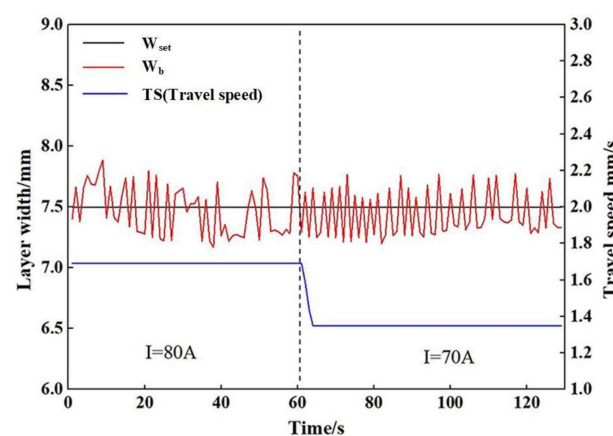


Figure 12. Closed-loop control under deposition current disturbance.

Figure 12 shows the control effect under the deposition current step test. It can be found that the initial width of the deposited layer is 7.5 mm. When the time reaches 60 s, the deposition current decreases from 80 A to 70 A. This reduction in current is due to the continuous arc during deposition, leading to heat accumulation and thermal inertia in the molten pool. With the significant decrease in the sedimentary current and speed, the width of the deposited layer experiences a change within the range of 2 to 4 s, ultimately

converging towards a specified width. Moreover, due to the inherent lag in the process of deposition, the control effect of the PSD on the deposited layer's width becomes apparent after a certain duration. Figure 12 shows a negative step in the current during deposition, and a decrease in deposition speed results in the deposited layer's width approaching a more consistent value. Notably, the data from the experiment show a lack of noticeable interference points, affirming the effectiveness and stability of the PSD control effect on the deposited layer.

Figure 13 shows the effect of PSD on controlling the thickness of the deposited layer. We set the total number of deposition layers to 10 and configure the length of each deposition layer as 85 mm. We collect thickness data for the fourth and fifth deposition layers separately. The fourth layer is the original deposition layer, and visual sensing detection is carried out after the deposition. The fifth layer is to make up for the defects of the fourth layer after PSD control. Figure 13 reveals an uneven surface on the fourth layer, with the thickness falling within the expected fluctuation range. This unevenness is attributed to adjustments in the wire feed speed, resulting in a higher wire feed rate per unit of time and subsequently increasing the thickness of the deposited layer after the molten pool solidifies, assuming all other process parameters remain constant. Furthermore, it is essential to recognize the substantial impact of the deposition current on regulating the deposition layer's dimensions, as supported by the data in Figure 9.

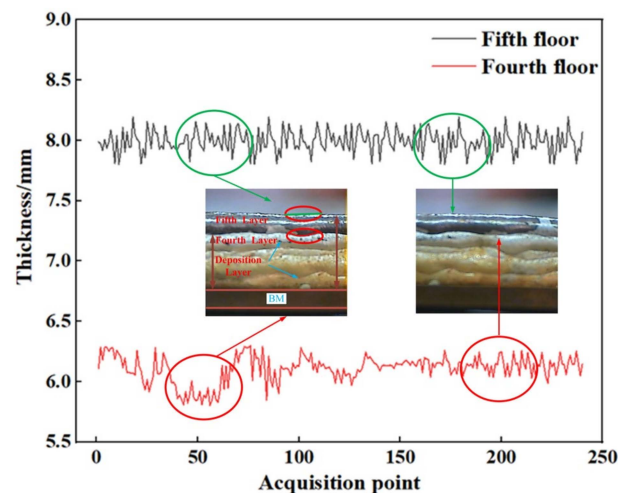


Figure 13. Layer width under control.

### 5.2. Adjustable Layer Width Control

For this research, the PSD algorithm is applied to the width control of robot GTA-AM thin-walled parts and then the thickness of the deposition layer is regulated. Therefore, under the condition of setting the same arc length, the process parameters are controlled to make the deposition size approximately consistent. If the width of the second layer remains within the range of 7.5 mm to 8.3 mm, it is preferable to set the width at 7.5 mm. Subsequently, the width of the next layer is controlled based on the width of the preceding layer. The PSD control algorithm is employed to fine-tune the deposition speed and the deposition current accordingly.

Figure 14 presents a visual representation of width detection and deposition speed across various cladding layers, demonstrating the impact of the closed-loop controller. In Figure 14, the black dashed line represents the height from the start to the end of the additive component, corresponding to the black numbers on the left side of the vertical axis. The red curve depicts the actual width values of the molten pool during the additive manufacturing process, corresponding to the red numbers on the vertical axis. The black straight line represents the predetermined value for the given deposition layer width, corresponding to the red numbers on the vertical axis. The blue dashed line indicates the movement speed, corresponding to the blue numbers on the vertical axis. When the width

of the molten pool is less than the predetermined value, the robot speed decreases; when the width of the molten pool is over than the predetermined value, the robot speed increases. Clearly, with precise control of the deposition parameters, the width of the deposited layer falls within the range of  $[-0.3, 0.3]$ . This effective control ensures that the width of the deposited layer remains within the specified limits. Moreover, the thickness growth pattern for each layer within the thin-walled structure follows a consistent trend, as highlighted in reference [39]. The data in Figure 14 reveal that the average variances for different layer widths and total thicknesses are calculated to be 0.2435 mm and 0.2482 mm, respectively.

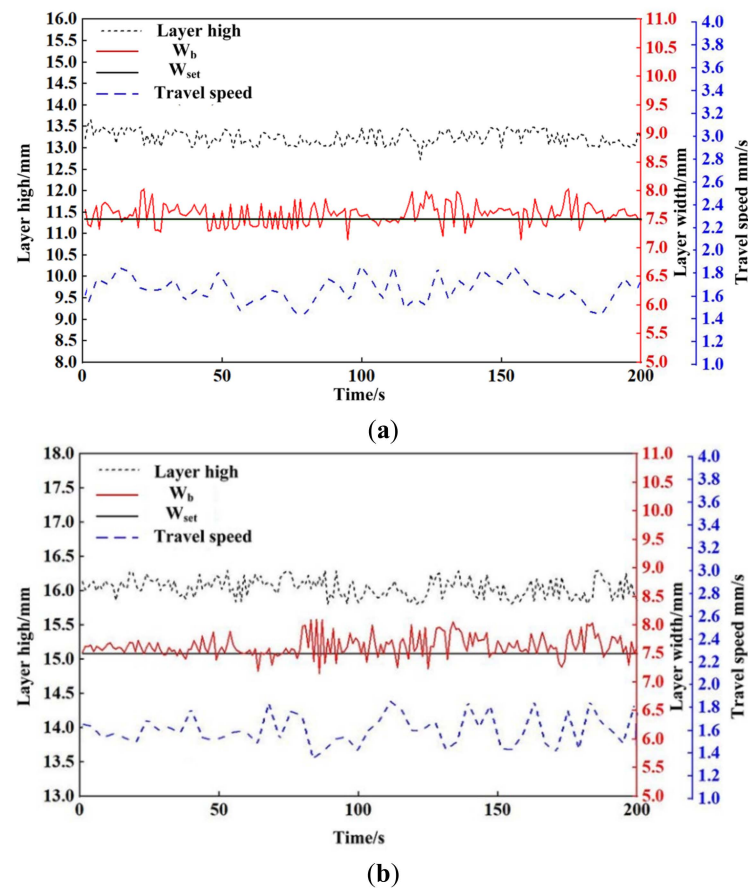


**Figure 14.** Single-layer multi-channel DED-Arc closed-loop control at a 1.0 mm step size: (a) layer 8; (b) layer 10.

The size change detection results of different layers in Figure 14 demonstrate effective control over the width of the deposited layer. Furthermore, deposition current and deposition speed influence the width of the deposited layer. It is noteworthy that this conclusion is obtained under the same conditions of other parameters. While maintaining other process parameters constant, the influence of the deposition speed on the height of the structural component is not substantial, but the impact of the deposition current is more pronounced. Based on this control mode, the thin-walled structural parts are shown in Figure 15.

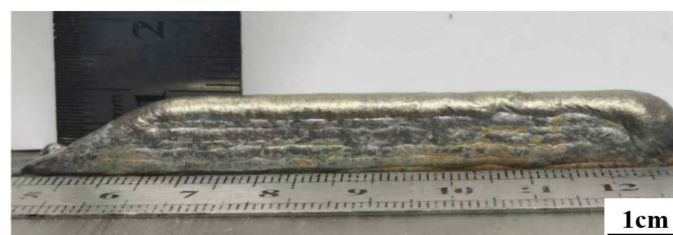


**Figure 15.** Deposition wall forming in the DED-Arc control process.

Through the implementation of the PSD control algorithm, we have observed a correlation between the selection of points between adjacent peaks in Figure 15 and the height of the sedimentary layer. As the number of deposition layers increases, the selected points increase layer by layer, showcasing a nearly consistent rise, as detailed in [40]. This relationship is influenced by the visual sensor's capability to capture the tungsten electrode's top and provide insights into the deposited layer's shape and the molten pool using a mirror. The observed sharpness in this context is approximately 10 mm.

In cases where the deposition speed is excessively slow while the deposition current is excessively high, the deposition layer becomes too large, causing the molten pool to flow excessively. This results in an extensive detection system and compromises control stability. Thus, we have identified an optimal layer width control range between 7.5 mm and 8.3 mm. Within this range, the height of the structural part remains relatively stable. The final form of the final thin-walled formation part is shown in Figure 16.



**Figure 16.** The final form of the thin-walled parts in the DED-Arc control process.

## 6. Conclusions

This study focused on the DED-Arc technique for thin-walled structural parts, specifically addressing width control during the deposition process. Additionally, the GTA-AM process was controlled to form thin-walled structural parts within a defined parameter range. The main conclusions obtained by this study are as follows:

1. The DED-Arc is a nonlinear procedure, and, in order to grasp the connection between deposition speed and deposited layer width, we have developed a second-order Hammerstein model. This model is crucial in shaping the height control mechanism for the structural components.
2. A PSD control strategy is introduced to regulate various deposited layers' widths. This method can ensure the maximum error between the detected actual package's width, determined by the vision sensor, and the desired cladding layer's width remains within 0.8 mm. Furthermore, the maximum pre-set cladding layer's width is effectively constrained, so as not to exceed 8.3 mm. This control strategy facilitates a stable, incremental trend in the cladding layer's height for these structural parts.
3. To maintain control effectiveness and stability, it is recommended to keep the width of the sedimentary layer within the range of 7.5 mm to 8.3 mm when utilizing the deposition speed as the control variable. This range ensures optimal control and stability in the fabrication process.

**Author Contributions:** Conceptualization, Z.W., S.Y. and D.F.; data curation, Q.W.; formal analysis, Y.X. and X.Y.; methodology, J.H. and S.Y.; supervision, J.H.; validation, D.F.; writing—original draft, Q.W.; writing—review and editing, Z.W., Y.X., J.H. and X.Y. All authors have read and agreed to the published version of the manuscript.



**Funding:** This work was financially supported by the National Natural Science Foundation of China (No. 52175324). The authors are grateful for the financial support from the Major Science and Technology Project of the Gansu Province (22ZD6GA008).

**Data Availability Statement:** The data presented in this study are available on request from the corresponding author (ethics).

**Conflicts of Interest:** The authors declare that they have no known competing financial interests or personal relationships that could have appeared to influence the work reported in this paper.

## References

1. Liu, D.; Lee, B.; Babkin, A.; Chang, Y. Research progress of arc additive manufacture technology. *Materials* **2021**, *14*, 1415. [\[CrossRef\]](#) [\[PubMed\]](#)
2. Rosli, N.A.; Alkahari, M.R.; bin Abdollah, M.F.; Maidin, S.; Ramli, F.R.; Herawan, S.G. Review on effect of heat input for wire arc additive manufacturing process. *J. Mater. Res. Technol.* **2021**, *11*, 2127–2145. [\[CrossRef\]](#)
3. Bi, J.; Wu, L.; Li, S.; Yang, Z.; Jia, X.; Starostenkov, M.D.; Dong, G. Beam shaping technology and its application in metal laser additive manufacturing: A review. *J. Mater. Res. Technol.* **2023**, *26*, 4606–4628. [\[CrossRef\]](#)
4. Duan, X.; Li, Q.; Xie, W.; Yang, X. Wire arc metal additive manufacturing using pulsed arc plasma (PAP-WAAM) for effective heat management. *J. Mater. Process. Technol.* **2023**, *311*, 117806. [\[CrossRef\]](#)
5. Treutler, K.; Wesling, V. The current state of research of wire arc additive manufacturing (WAAM): A review. *Appl. Sci.* **2021**, *11*, 8619. [\[CrossRef\]](#)
6. Duarte, V.R.; Rodrigues, T.A.; Schell, N.; Miranda, R.M.; Oliveira, J.P.; Santos, T.G. In-situ hot forging directed energy deposition-arc of CuAl8 alloy. *Addit. Manuf.* **2022**, *55*, 102847. [\[CrossRef\]](#)
7. Cunningham, C.R.; Dhokia, V.; Shokrani, A.; Newman, S.T. Effects of in-process LN2 cooling on the microstructure and mechanical properties of type 316L stainless steel produced by wire arc directed energy deposition. *Mater. Lett.* **2021**, *282*, 128707. [\[CrossRef\]](#)
8. Farias, F.W.C.; Duarte, V.R.; Felice, I.O.; da Cruz Payao Filho, J.; Schell, N.; Maawad, E.; Avila, J.A.; Li, J.Y.; Zhang, Y.; Santos, T.G.; et al. In situ interlayer hot forging arc-based directed energy deposition of Inconel® 625: Process development and microstructure effects. *Addit. Manuf.* **2023**, *66*, 103476. [\[CrossRef\]](#)
9. Scheck, M.; Richter, A.; Beitler, S.; Gehling, T.; Treutler, K.; Wesling, V.; Rembe, C.; Bohn, C. High geometric fidelity through closed-loop control of the weld pool size in gas metal arc welding based direct energy deposition. *Addit. Manuf.* **2024**, *80*, 103944. [\[CrossRef\]](#)
10. Xiong, J.; Wen, C. Arc plasma, droplet, and forming behaviors in bypass wire arc-directed energy deposition. *Addit. Manuf.* **2023**, *70*, 103558. [\[CrossRef\]](#)
11. Xiong, J.; Zhang, G.; Hu, J.; Wu, L. Bead geometry prediction for robotic GMAW-based rapid manufacturing through a neural network and a second-order regression analysis. *J. Intell. Manuf.* **2014**, *25*, 157–163. [\[CrossRef\]](#)
12. Abranovic, B.; Sarkar, S.; Chang-Davidson, E.; Beuth, J. Melt pool level flaw detection in laser hot wire directed energy deposition using a convolutional long short-term memory autoencoder. *Addit. Manuf.* **2024**, *79*, 103843. [\[CrossRef\]](#)
13. Wang, Q.; Li, J.; Gouge, M.; Nassar, A.R.; Michaleris, P.; Reutzel, E.W. Physics-based multivariable modeling and feedback linearization control of melt-pool geometry and temperature in directed energy deposition. *J. Manuf. Sci. Eng.* **2017**, *139*, 021013. [\[CrossRef\]](#)
14. Wu, B.; Pan, Z.; Chen, G.; Ding, D.; Yuan, L.; Cuiuri, D.; Li, H. Mitigation of thermal distortion in wire arc additively manufactured Ti6Al4V part using active interpass cooling. *Sci. Technol. Weld. Join.* **2019**, *24*, 484–494. [\[CrossRef\]](#)
15. Chen, X.; Wang, C.; Ding, J.; Qu, R.; Wang, Y.; Pardal, G.; Williams, S. Thermal fluid dynamics of the effect of filler wire on deposition rate and bead formation intending plasma arc-based DED. *J. Manuf. Process.* **2023**, *107*, 199–209. [\[CrossRef\]](#)
16. Shi, J.; Li, F.; Chen, S.; Zhao, Y.; Tian, H. Effect of in-process active cooling on forming quality and efficiency of tandem GMAW-based additive manufacturing. *Int. J. Adv. Manuf. Technol.* **2019**, *101*, 1349–1356. [\[CrossRef\]](#)
17. Dezaki, M.L.; Serjouei, A.; Zolfagharian, A.; Fotouhi, M.; Moradi, M.; Ariffin, M.K.A.; Bodaghi, M. A review on additive/subtractive hybrid manufacturing of directed energy deposition (DED) process. *Adv. Powder Mater.* **2022**, *1*, 100054. [\[CrossRef\]](#)
18. Zhang, S.; Zhang, Y.; Gao, M.; Wang, F.; Li, Q.; Zeng, X. Effects of milling thickness on wire deposition accuracy of hybrid additive/subtractive manufacturing. *Sci. Technol. Weld. Join.* **2019**, *24*, 375–381. [\[CrossRef\]](#)
19. Dávila, J.L.; Neto, P.I.; Noritomi, P.Y.; Coelho, R.T.; da Silva, J.V.L. Hybrid manufacturing: A review of the synergy between directed energy deposition and subtractive processes. *Int. J. Adv. Manuf. Technol.* **2020**, *110*, 3377–3390. [\[CrossRef\]](#)
20. Spencer, J.D.; Dickens, P.M.; Wykes, C.M. Rapid prototyping of metal parts by three-dimensional welding. *Proc. Inst. Mech. Eng. Part B J. Eng. Manuf.* **1998**, *212*, 175–182. [\[CrossRef\]](#)
21. Colegrove, P.A.; Coules, H.E.; Fairman, J.; Martina, F.; Kashoob, T.; Mamash, H.; Cozzolino, L.D. Microstructure and residual stress improvement in wire and arc additively manufactured parts through high-pressure rolling. *J. Mater. Process. Technol.* **2013**, *213*, 1782–1791. [\[CrossRef\]](#)
22. Karunakaran, K.P.; Suryakumar, S.; Pushpa, V.; Akula, S. Low cost integration of additive and subtractive processes for hybrid layered manufacturing. *Robot. Comput. Integr. Manuf.* **2010**, *26*, 490–499. [\[CrossRef\]](#)

23. Doumanidis, C.; Kwak, Y.M. Multivariable adaptive control of the bead profile geometry in gas metal arc welding with thermal scanning. *Int. J. Press. Vessel. Pip.* **2002**, *79*, 251–262. [[CrossRef](#)]
24. Xiong, J.; Zhang, G. Online measurement of bead geometry in GMAW-based additive manufacturing using passive vision. *Meas. Sci. Technol.* **2013**, *24*, 115103. [[CrossRef](#)]
25. Herali , A.; Christiansson, A.K.; Lennartson, B. Height control of laser metal-wire deposition based on iterative learning control and 3D scanning. *Opt. Lasers Eng.* **2012**, *50*, 1230–1241. [[CrossRef](#)]
26. Fan, H.; Ravala, N.K.; Wickle, H.C., III; Chin, B.A. Low-cost infrared sensing system for monitoring the welding process in the presence of plate inclination angle. *J. Mater. Process. Technol.* **2003**, *140*, 668–675. [[CrossRef](#)]
27. Smith, J.S.; Balfour, C. Real-time top-face vision based control of weld pool size. *Ind. Robot Int. J.* **2005**, *32*, 334–340. [[CrossRef](#)]
28. Liu, Y.K.; Zhang, Y.M. Model-based predictive control of weld penetration in gas tungsten arc welding. *IEEE Trans. Control Syst. Technol.* **2013**, *22*, 955–966. [[CrossRef](#)]
29. Liu, Y.K.; Zhang, Y.M. Control of 3D weld pool surface. *Control Eng. Pract.* **2013**, *21*, 1469–1480. [[CrossRef](#)]
30. Zhang, C.; Gao, M.; Chen, C.; Zeng, X. Spectral diagnosis of wire arc additive manufacturing of Al alloys. *Addit. Manuf.* **2019**, *30*, 100869. [[CrossRef](#)]
31. Kim, S.; Jeon, I.; Sohn, H. Infrared thermographic imaging based real-time layer height estimation during directed energy deposition. *Opt. Lasers Eng.* **2023**, *168*, 107661. [[CrossRef](#)]
32. H lscher, L.V.; Hassel, T.; Maier, H.J. Detection of the contact tube to working distance in wire and arc additive manufacturing. *Int. J. Adv. Manuf. Technol.* **2022**, *120*, 989–999. [[CrossRef](#)]
33. Chabot, A.; Rauch, M.; Hasco t, J.Y. Novel control model of Contact-Tip-to-Work Distance (CTWD) for sound monitoring of arc-based DED processes based on spectral analysis. *Int. J. Adv. Manuf. Technol.* **2021**, *116*, 3463–3472. [[CrossRef](#)]
34. Li, F.; Chen, S.; Wu, Z.; Yan, Z. Adaptive process control of wire and arc additive manufacturing for fabricating complex-shaped components. *Int. J. Adv. Manuf. Technol.* **2018**, *96*, 871–879. [[CrossRef](#)]
35. Fathi, A.; Khajepour, A.; Toyserkani, E.; Durali, M. Clad height control in laser solid freeform fabrication using a feedforward PID controller. *Int. J. Adv. Manuf. Technol.* **2007**, *35*, 280–292. [[CrossRef](#)]
36. Xiong, J.; Yin, Z.; Zhang, W. Closed-loop control of variable layer width for thin-walled parts in wire and arc additive manufacturing. *J. Mater. Process. Technol.* **2016**, *233*, 100–106. [[CrossRef](#)]
37. Marsik, J. A new conception of digital adaptive PSD control. *Probl. Control Inf. Theory* **1983**, *12*, 267–279.
38. Hartmann, T.; Keck, F.; Korsch, H.J.; Mossmann, S. Dynamics of Bloch oscillations. *New J. Phys.* **2004**, *6*, 2. [[CrossRef](#)]
39. Guo, H.; Zhao, N.; Yang, H.; Li, S.; Zheng, H. Analysis on stationary window of oblique detonation wave in methane-air mixture. *Aerosp. Sci. Technol.* **2021**, *118*, 107038. [[CrossRef](#)]
40. Zhao, T.; Lv, X.; Zhang, H.; Zhang, S. Wireless ultraviolet scattering channel estimation method based on deep learning. *Opt. Express* **2021**, *29*, 39633–39647. [[CrossRef](#)]

**Disclaimer/Publisher’s Note:** The statements, opinions and data contained in all publications are solely those of the individual author(s) and contributor(s) and not of MDPI and/or the editor(s). MDPI and/or the editor(s) disclaim responsibility for any injury to people or property resulting from any ideas, methods, instructions or products referred to in the content.